ELSEVIER

Contents lists available at ScienceDirect

# **Atmospheric Environment**

journal homepage: www.elsevier.com/locate/atmosenv



# Impact of the Knudsen number and mass-transfer expression on multi-phase kinetic modeling

Prasad Pokkunuri a,b, Paul Nissenson b, Donald Dabdub b,\*

- <sup>a</sup> University of California, Irvine, Department of Chemistry, Irvine, CA 92697-2025, USA
- <sup>b</sup> University of California, Irvine, Department of Mechanical and Aerospace Engineering, Irvine, CA 92697-3975, USA

#### ARTICLE INFO

Article history: Received 21 May 2009 Received in revised form 8 October 2009 Accepted 14 October 2009

Keywords: Knudsen number Mass-transfer coefficient Interfacial reaction Multi-phase kinetics

#### ABSTRACT

Three different mass-transfer expressions are employed within the Model of Aerosol, Gas, and Interfacial Chemistry (MAGIC) to study gas-phase molecular chlorine and bromine production from NaCl and NaBr aerosols, respectively. Simulations of chamber experiments are performed in which NaCl aerosols react with gas-phase ozone in the presence of UV light, in order to identify the importance of the Knudsen number and mass-transfer expression in systems with varying contributions from gas-phase, aqueousphase, and interfacial chemistry. In the case of NaBr aerosols, simulations are performed of both dark and photolytic conditions. A range of Knudsen numbers spanning the continuum, transition and freemolecular regimes is studied. Particle size is varied over three orders of magnitude, and particle concentration is changed to keep either (a) total aerosol volume or (b) total aerosol surface area constant. When total aerosol volume is constant, the total amount of surface area available for interfacial reaction increases linearly with Knudsen number. Consequently peak gas-phase Cl2 and Br2 concentrations increase by two orders of magnitude from the continuum regime to the free-molecular regime. When total aerosol surface area is constant, total aerosol volume is inversely proportional to Knudsen number, with lesser volume being available at higher Knudsen numbers. Consequently Cl<sup>-</sup> depletion in the kinetic regime leads to most gas-phase Cl<sub>2</sub> being produced in the transition regime. Gas-phase Br<sub>2</sub> concentration trends are determined by aqueous-phase reaction mechanisms, leading to a monotonic decrease in production with Knudsen number. At all Knudsen numbers, more gas-phase bromine is produced in the photolytic case than in the dark case, the difference being significant in the transition regime. Results of this study suggest that halogen production is insensitive to the mass-transfer expression used in the simulations.

© 2009 Elsevier Ltd. All rights reserved.

#### 1. Introduction

Detailed models of atmospheric systems include non-equilibrium kinetics, with interactions between gaseous and aqueousphases. Although such detailed models are intractable when used in large three-dimensional simulations, valuable insight is gleaned into important processes of atmospheric relevance. For example, Knipping et al. (2000) obtained evidence for interfacial reactions occurring on the surface of aerosol particles using the MAGIC model (Model of Aerosol, Gaseous, and Interfacial Chemistry). Knipping et al. (2000) and subsequent studies (Hunt et al., 2004; Thomas et al., 2006, 2007) have shown that far greater amounts of gaseous Cl<sub>2</sub> and Br<sub>2</sub> are released into the gas-phase due to interfacial reactions than is possible from reactions in the gas-phase or

aqueous-phase when considering deliquesced NaCl and NaBr particles respectively. Chlorine chemistry is important in ozone production via photochemical reactions involving VOCs and  $NO_x$  in coastal regions since VOCs,  $NO_x$ , and sea-salt particles are all present in significant concentrations here (Knipping and Dabdub, 2003). Over the open ocean, in the remote marine boundary layer, and in polar regions, halogen chemistry plays an important role in ozone destruction (Foster et al., 2001; Piot and von Glasow, 2008; Read et al., 2008). In all these regions, sea-salt aerosol is present in the marine boundary layer at relative humidities well over the deliquescence point. The interfacial reactions examined in the above studies are the following:

$$OH_{(g)} + Cl_{surface}^{-} \rightarrow 0.5Cl_{2(g)} + OH_{(aq)}^{-}$$
 (1)

$$OH_{(g)} + Br_{surface}^{-} \rightarrow 0.5Br_{2(g)} + OH_{(aq)}^{-}$$
 (2)

$$O_{3(g)} + Br_{surface}^- \rightarrow 0.5Br_{2(g)} + O_{3(aq)}^-.$$
 (3)

<sup>\*</sup> Corresponding author. Tel.: +1 949 824 6126; fax: +1 949 824 8585. E-mail address: ddabdub@uci.edu (D. Dabdub).

The hydroxyl radical in the first two reactions is generated by the photolysis of ozone (Finlayson-Pitts and Pitts, 2000),

$$O_{3(g)} + h\nu \rightarrow O(^{1}D)_{(g)} + O_{2(g)}$$
 (4)

$$O(^{1}D)_{(g)} + H_{2}O_{(g)} \rightarrow 2OH_{(g)}.$$
 (5)

Reactions (4) and (5) occur only during photolytic conditions, i. e., when ozone is exposed to a UV light source. Reaction with ozone on the surface of NaBr particles presents an alternate route for  $\text{Br}_{2(g)}$  to be released from aerosols and may be a significant source of bromine in the dark when  $\text{OH}_{(g)}$  is not available. The interface reactions, as represented above, constitute the net outcome of a process that most likely involves one or more intermediates.

Any multi-phase kinetics model in general, and MAGIC in particular, consists of numerous gaseous and aqueous reaction rate constants representing chemistry in the respective phases, Henry's law constants and mass accommodation coefficients used in determining mass-transfer rates between the phases, and parameters to calculate interfacial reaction rates. In situations that are of atmospheric relevance, it is likely that the gaseous and aqueousphases are not in equilibrium. As a result, non-equilibrium expressions are used to define the rate of mass transfer between the phases. In many atmospheric models, such as those described in Jacob (2000) and von Glasow et al. (2002), the mass-transfer expression due to Schwartz (1986) is used due to its simplicity, both conceptually and computationally. There have been limited studies that use other mass-transfer expressions, for example Pandis and Seinfeld (1989), but none of them compare results using different mass-transfer expressions. The studies that compare mass-transfer expressions often are limited in scope. For instance, Sander (1999) compared values of the mass-transfer coefficient,  $k_{\rm mt}$ , obtained using two different expressions, but did not include them in an atmospherically relevant model.

The present work is aimed at implementing different mass-transfer expressions in a detailed chemical kinetics model of atmospheric relevance. For this purpose, three expressions for the mass-transfer coefficient, developed by Fuchs (1964), Fuchs and Sutugin (1971), and Schwartz (1986), are implemented in MAGIC and are used to study the production of gas-phase molecular chlorine and bromine from deliquesced NaCl and NaBr particles respectively. Since exact rate expressions for the interfacial reactions (1)–(3) are not known, the interfacial reaction rates are calculated based on rates of mass-transfer to the interface. This approach also is adopted by Jacob (2000) and Thomas et al. (2006, 2007). Since interfacial reaction rates depend on the mass-transfer rate using this approach, the importance of using a detailed, physically sound model to represent inter-phase mass transfer is enhanced greatly.

This paper is organized as follows. In the next section, a description of the problem is provided by introducing and explaining the three mass-transfer expressions. The various situations considered to compare the three mass expressions are discussed in Section 3. Results are presented and discussed in Section 4. Finally, conclusions and atmospheric implications are provided in Section 5.

#### 2. Problem description

In general, a non-equilibrium, multi-phase kinetics model should account for the following physical and chemical processes: (i) gas-phase diffusion and chemical reactions; (ii) aqueous-phase diffusion and chemical reactions; (iii) interfacial mass transport; and (iv) interfacial reactions, if any. MAGIC includes detailed submodels for each of the above processes. The model was developed

to simulate time evolution of chemical species in the gas- and aqueous-phases for reactions of NaCl and NaBr particles in the presence of ozone in an enclosed chamber. The chamber design, experiments, and MAGIC are described in detail elsewhere (Oum et al., 1998; DeHaan et al., 1999; Knipping et al., 2000; Knipping and Dabdub, 2002; Hunt et al., 2004). The model includes a total of 24 gas-phase and 44 aqueous-phase species, whose concentrations are governed by the following equations (Thomas et al., 2006, 2007):

$$\frac{\partial C_{\rm g}}{\partial t} = R_{\rm g} \pm \omega R_{\rm int} - \omega k_{\rm mt} \left( C_{\rm g} - \frac{C_{\rm aq}}{\rm HRT} \right)$$
 (6)

$$\frac{\partial C_{aq}}{\partial t} = R_{aq} \mp R_{int} + k_{mt} \left( C_g - \frac{C_{aq}}{HRT} \right), \tag{7}$$

where  $C_{\rm g}$  (molecules cm<sup>-3</sup>) and  $C_{\rm aq}$  (mol L<sup>-1</sup>) represent species concentration in the gas- and aqueous-phases respectively, t denotes time,  $R_{\rm g}$ ,  $R_{\rm aq}$ , and  $R_{\rm int}$  (concentration s<sup>-1</sup>) denote chemical reaction rates in the gas-phase, aqueous-phase and at the interface respectively,  $k_{\rm mt}$  (s<sup>-1</sup>) is the mass-transfer coefficient, H (M atm<sup>-1</sup>) is the effective Henry's law constant, R is the universal gas constant, T is the absolute temperature (298 K), and  $\omega$  is a dimensionless ratio representing the volumetric aqueous aerosol liquid water mixing ratio. Species concentrations, as a function of time, are obtained by solving the coupled system of differential equations simultaneously for each of the gas-phase and aqueous-phase species involved.

#### 2.1. Mass transport between the phases

In MAGIC, 15 species are transported between the gas- and aqueous-phases across the aerosol surface. For these species, interfacial mass transport is described by the use of a mass-transfer coefficient,  $k_{\rm mt}$ . The mass-transfer coefficient is a first-order rate coefficient that combines first-order rates of gas-phase diffusion to the aerosol surface and kinetic, or 'free-molecular', transport across the aerosol surface.

Gas-phase diffusion far away from aerosol particles is governed by continuum transport. Closer to the particles, however, a continuum assumption is no longer universally valid and size of the particles relative to the mean free path of the gas-phase molecules must be considered. When the particle radius (r) is of the same order as the mean free path  $(\lambda)$  of the gas-phase molecules, the transition regime is in effect. In this regime, species concentration distributions are governed rigorously by the Boltzmann equation for which a general solution does not exist. To avoid solving the Boltzmann equation directly, an approach based on flux-matching is used. Non-continuum effects are assumed to be limited to a small spherical region of thickness  $\Delta$  around the particle. This thickness  $(\Delta)$  is of the order of the mean free path and the kinetic theory of gases is assumed to apply in this region. Three mass-transfer expressions based on different flux-matching schemes, which use the same definition of the mean free path,  $\lambda = 3D_g/\overline{\nu}$ , are employed in this study.

Schwartz (1986) derived an expression for the mass transport coefficient by assuming that at the droplet surface, transport suddenly switches from the continuum regime to the kinetic regime, implementing a flux-matching at the droplet surface ( $\Delta=0$ ). In this scenario, the mass-transfer coefficient is,

$$k_{\rm mt}^{\rm Sch} = \left(\frac{r^2}{3D_{\rm g}} + \frac{4r}{3\overline{\nu}\alpha}\right)^{-1},\tag{8}$$

where  $D_{\rm g}~({\rm cm}^2~{\rm s}^{-1})$  is the gas-phase diffusivity,  $\bar{\nu}~({\rm cm}~{\rm s}^{-1})$  is the mean molecular speed, and  $\alpha$  (dimensionless) is the mass accommodation coefficient.

Fuchs and Sutugin (1971) used a different approach, fitting Sahni's (1966) solution to the Boltzmann equation, to obtain a different expression for the mass-transfer coefficient,

$$k_{\rm mt}^{\rm FS} = \frac{\lambda \overline{v}}{\left(1 + \left(\lambda_{\rm Sa} + 4\frac{1 - \alpha}{3\alpha}\right)\frac{\lambda}{r}\right)r^2},\tag{9}$$

where  $\lambda_{Sa}$  is a dimensionless number adopted from Sahni (1966),

$$\lambda_{Sa} \approx \frac{4/3 + 0.71r/\lambda}{1 + r/\lambda}.\tag{10}$$

Following Fuchs (1964), who originally suggested the flux-matching approach, yet another expression is obtained for the mass-transfer coefficient.

$$k_{\rm mt}^{\rm Fuchs} = \left(\frac{r^2}{3D_{\rm g}\left(1 + Kn\frac{\Delta}{\lambda}\right)} + \frac{4r}{3\bar{\nu}\alpha}\right)^{-1}.$$
 (11)

Here  $Kn = \lambda/r$  is the Knudsen number, a non-dimensional ratio. Note that the Schwartz expression, Equation (8), can be obtained from the Fuchs expression, Equation (11), by making the substitution  $\Delta = 0$ . Interestingly, Fuchs (1964) originally suggested  $\Delta = 0$ .

The mass-transfer expression due to Fuchs and Sutugin (1971), Equation (9), can also be written in a form analogous to Equations (8) and (11) as follows:

$$k_{\rm mt}^{\rm FS} = \left(\frac{r^2}{3D_{\rm g}} \left(1 - \frac{0.62}{1 + r/\lambda}\right) + \frac{4r}{3\overline{\nu}\alpha}\right)^{-1}.$$
 (12)

Pandis and Seinfeld (1989) presented  $k_{\rm mt}^{\rm FS}$  in an alternate way, as a product of the continuum mass-transfer coefficient and a correction factor as  $k_{\rm mt}^{\rm FS} = \frac{3D_x}{r^2}\eta$ . Seinfeld and Pandis (1998), in their review of the flux–matching problem, presented similar correction factors for other flux–matching approaches.

Equation (8) is used in many atmospheric models, e.g. Jacob (2000) and von Glasow et al. (2002). Pandis and Seinfeld (1989) used the Fuchs and Sutugin expression, Equation (9). Sander (1999) concluded that  $k_{\rm mt}^{\rm Fc}$  is always larger than  $k_{\rm mt}^{\rm Sch}$ , the relative difference being no more than 15% and significant only around Kn=1 which constitutes the transition regime. MAGIC however, solves a system of non-linear, coupled differential equations and a small change in some parameters could lead to a large change in the output. The effect of using different mass-transfer expressions on the output can be known only by implementing them in the model and comparing the results obtained.

#### 2.2. Interface reaction rates

Mass accommodation and interface chemistry are inherently coupled processes. A few of the 15 species that are transported across the interface also are involved in surface reactions (1)–(3). Since exact rate expressions for these complex interface processes are unknown, atmospheric modelers calculate interfacial reaction rates based on the amount of molecules transferring between the gas- and aqueous-phases and the propensity for surface reaction with ions present at the interface. MAGIC uses a modified version of the resistor model discussed in Hu et al. (1995) to account for competition between surface reactions and mass accommodation. Interface reactions are given preference over mass accommodation and the two processes are allowed to occur in parallel. The interfacial reaction rate, being closely related to the rate of mass transport between the phases, depends on the mass-transfer coefficient used. Expressed in terms of aqueous-phase product

formed, the interfacial reaction rate using the Schwartz masstransfer coefficient Equation (8) is,

$$R_{\rm int} = \left(\frac{r^2}{3D_{\rm g}} + \frac{4r}{3\overline{\nu}\gamma}\right)^{-1} \left[A_{\rm (g)}\right],\tag{13}$$

where

$$\gamma = \phi \gamma' \beta_X \left[ X_{\text{surf}}^{-} \right]. \tag{14}$$

is the overall surface reaction probability,  $\beta_X[X_{\text{surf}}]$  is the fraction of droplet surface covered by ions that have reached the interface,  $\phi$  is the average number of contacts between  $A_{(g)}$  and  $X_{\text{surf}}^-$ , and  $\gamma'$  denotes the probability that  $X^-$  and  $A_{(g)}$  will react when these species come in contact. Here  $X^-$  and  $A_{(g)}$  represent any of the surface ion and gas-phase molecule pairs that react at the interface reactions (1)–(3). The quantity  $\gamma'$ , being a probability, can theoretically vary from 0 to 1. Values for  $\gamma'$  are chosen following sensitivity studies of NaCl and NaBr aerosols presented by Nissenson et al. (2008, 2009).

The interfacial reaction rate (Equation 13) is computed as a product of gas-phase concentration and a coefficient obtained from the relevant mass-transfer coefficient, Equation (8) in this case, by replacing mass accommodation coefficient  $\alpha$  with surface reaction probability  $\gamma$ . Interface reaction rates using the other two mass-transfer expressions, Equations (9) and (11), are obtained in an identical fashion.

To account for interfacial reaction being preferred over non-reactive uptake, mass accommodation coefficients for O<sub>3</sub> and OH, which undergo both processes simultaneously, are modified as follows:

$$\alpha' = \alpha(1 - \gamma). \tag{15}$$

In addition to the interfacial processes listed above, gaseous bromine also may undergo irreversible uptake by chamber walls. The first-order rate constant for this process is determined from experiments described in Hunt et al. (2004).

In summary, three mass-transfer expressions have been described and the corresponding interfacial reaction rates derived. The mass-transfer coefficients depend on known particle properties such as particle radius r, and gas-phase properties such as diffusivity  $D_{\rm g}$ , mass accommodation coefficient  $\alpha$ , and mean molecular speed  $\bar{\nu}$  which vary with species. The Fuchs mass-transfer expression, Equation (11), depends on an additional quantity  $\Delta$ , the distance from the particle surface at which flux-matching is performed. This quantity is a parameter that needs to be determined.

#### 3. Methodology

The three mass-transfer expressions described in the previous section are implemented in MAGIC. Simulations are performed of chamber experiments in which deliquesced NaCl and NaBr particles react with ozone in the presence of UV light. These experiments are described in detail elsewhere (Oum et al., 1998; Knipping et al., 2000; Hunt et al., 2004). The Fuchs mass-transfer expression, Equation (11), has a parameter  $\Delta$  whose value must be selected. In preliminary studies, gas-phase chlorine and bromine concentration profiles are compared for different values of the parameter  $\Delta$ . These concentration profiles show the same qualitative behavior for all the values of  $\Delta$  studied. Supplementary Figs. 1 and 2 show gas-phase chlorine and bromine concentration profiles for 4 different values of  $\Delta$ . These simulations are performed at a transition range Knudsen number, Kn = 0.6. Peak gas-phase chlorine concentration

changes by about 14% between  $\Delta=0$  and  $\Delta=4$ . Gas-phase bromine concentration profiles, on the other hand, are insensitive to the value of  $\Delta$ . Additional simulations performed at free-molecular and continuum regime Knudsen numbers (not presented here) show both gas-phase chlorine and bromine concentration profiles to be insensitive to the value of  $\Delta$ .

Flux-matching theory requires  $\Delta$  to be of the order of the mean free path  $\lambda$  (Seinfeld and Pandis, 1998). With  $\Delta=0$ , the Schwartz expression, Equation (8), is recovered. Hence the value  $\Delta=\lambda$  is chosen in all further simulations using the Fuchs mass-transfer expression. Peak gas-phase chlorine concentrations differ by about 6% between  $\Delta=0$  and  $\Delta=1$ .

A range of Knudsen numbers  $0.01 \le Kn \le 10$  spanning the continuum, free-molecular and transition regimes of gas-phase transport is studied. Varying the Knudsen number over three orders of magnitude results in particle diameters varying approximately between 0.01 μm and 10 μm. Most atmospheric particles fall within this range of sizes. Total aerosol volume and total aerosol surface area in the system also vary over this range of particle diameters, affecting the relative importance of bulk processes like aqueous-phase chemistry and surface processes such as interfacial chemistry and mass transfer. To establish a basis for comparison, two types of analyses are performed in which the particle concentration is varied to keep (a) total aerosol volume and (b) total aerosol surface area constant. By varying total aerosol surface area, contributions from aqueous-phase chemistry to halogen production are constant. By varying total aerosol volume, the total aerosol surface area available for mass transfer and interface chemistry is constant. Tables 1 and 2 summarize particle sizes and concentrations for the range of Knudsen numbers examined, at constant total aerosol volume and constant total aerosol surface area respectively.

Peak  $\text{Cl}_{2(g)}$  in the case of NaCl particles and peak  $\text{Br}_{2(g)}$  in the case of NaBr particles are compared using the three different expressions introduced in Section 2.1. Simulations are performed of NaCl particles in the presence of  $O_{3(g)}$  under photolytic conditions, i.e., when irradiated by UV light. For NaBr particles, simulations are performed of both dark and photolytic conditions. In the dark, interfacial reaction (2) is absent and hence all the surface area is available for interfacial reaction (3) between  $\text{Br}_{\text{surface}}^{\text{curface}}$  and  $O_{3(g)}$ . Under photolytic conditions, both interfacial reactions compete for  $O_{3(g)}$ . This behavior is examined over a range of Knudsen numbers.

# 4. Results and discussion

## 4.1. Comparison of time evolution of $[Cl_{2(g)}]$

Time evolution of gas-phase  $\text{Cl}_2$  is studied at Knudsen numbers and particle concentrations reported in Tables 1 and 2. Fig. 1 shows

**Table 1**Particle sizes and concentrations of NaCl aerosol for the Knudsen numbers investigated. Particle concentration is changed to keep liquid water content (total amount of aerosol) in the system constant.

Knudsen number	Average particle median diameter (m)	Particle concentration (number m <sup>-3</sup> )	Comments
0.01	$1.30 \times 10^{-05}$	$9.67 \times 10^{+05}$	Continuum
0.05	$2.60 \times 10^{-06}$	$1.21 \times 10^{+08}$	regime
0.10	$1.30 \times 10^{-06}$	$9.67 \times 10^{+08}$	
0.25	$5.21 \times 10^{-07}$	$1.51 \times 10^{+10}$	
0.50	$2.60 \times 10^{-07}$	$1.21 \times 10^{+11}$	Transition
0.58	$2.24 \times 10^{-07}$	$1.86 \times 10^{+11}$	regime
0.75	$1.74 \times 10^{-07}$	$4.08 \times 10^{+11}$	
1.00	$1.30 \times 10^{-07}$	$9.67 \times 10^{+11}$	
2.00	$6.51 \times 10^{-08}$	$7.74 \times 10^{+12}$	Kinetic
5.00	$2.60 \times 10^{-08}$	$1.21 \times 10^{+14}$	regime
10.00	$1.30 \times 10^{-08}$	$9.67 \times 10^{+14}$	

**Table 2**Particle sizes and concentrations of NaCl aerosol for the Knudsen numbers investigated. Particle concentration is changed to keep total aerosol surface area in the system constant.

Knudsen number	Average particle median diameter (m)	Particle concentration (number m <sup>-3</sup> )	Comments
0.01	$1.30 \times 10^{-05}$	$5.62 \times 10^{+07}$	Continuum
0.05	$2.60 \times 10^{-06}$	$1.41 \times 10^{+09}$	regime
0.10	$1.30 \times 10^{-06}$	$5.62 \times 10^{+09}$	
0.25	$5.21 \times 10^{-07}$	$3.51 \times 10^{+10}$	
0.50	$2.60 \times 10^{-07}$	$1.41 \times 10^{+11}$	Transition
0.58	$2.24 \times 10^{-07}$	$2.02 \times 10^{+11}$	regime
0.75	$1.74 \times 10^{-07}$	$3.16 \times 10^{+11}$	
1.00	$1.30 \times 10^{-07}$	$5.62 \times 10^{+11}$	
2.00	$6.51 \times 10^{-08}$	$2.25 \times 10^{+12}$	Kinetic
5.00	$2.60 \times 10^{-08}$	$1.41 \times 10^{+13}$	regime
10.00	$1.30 \times 10^{-08}$	$5.62 \times 10^{+13}$	

 $\text{Cl}_{2(g)}$  concentration profiles computed using the three mass-transfer expressions, at the lowest, intermediate, and highest values of the Knudsen number, which represent the continuum, transition, and kinetic regimes respectively. There is a sharp rise in  $[\text{Cl}_{2(g)}]$  observed in all simulations when photolysis is initiated at 600 s.

#### 4.1.1. Constant total aerosol volume

When total aerosol volume is held constant, total aerosol surface area increases linearly with Kn, increasing the interface reaction rate at higher Knudsen numbers. This results in  $[\operatorname{Cl}_{2(g)}]$  increasing by two orders of magnitude from a peak value of about 0.2 ppbv at Kn=0.01 (Fig. 1a) to a peak value of about 70 ppbv at Kn=0.60 (Fig. 1c). The further increase to a peak of 130 ppbv at Kn=10.00, however, is not as dramatic.

The difference in peak  $[\operatorname{Cl}_{2(g)}]$  obtained in the three regimes is a direct consequence of the variation in surface area with Knudsen number. In both the transition and kinetic regime plots (Fig. 1c and e) this is seen as a sharp rise in  $[\operatorname{Cl}_{2(g)}]$  leading to the peak value and a subsequent less-steep fall as the available  $O_3$  is consumed by photolysis and  $\operatorname{Cl}_{2(g)}$  is lost to the walls and taken up by aerosols. At lower Knudsen numbers the interface reaction has lower available surface area on which to occur.  $\operatorname{Cl}_{2(g)}$  concentration rises slowly at the lowest Knudsen number (Fig. 1a) because the interfacial reaction occurs at a much slower rate than at the higher Knudsen numbers. Hydroxyl radicals react rapidly with other gas-phase species and are not able to produce  $\operatorname{Cl}_{2(g)}$  via interfacial reaction (1) in large quantities. This demonstrates the dominance of the interfacial reaction mechanism in producing gas-phase  $\operatorname{Cl}_2$  at all Knudsen numbers.

To determine whether peak  $[\operatorname{Cl}_{2(g)}]$  is limited by the  $O_3$  available for photolysis to  $\operatorname{OH}_{(g)}$ , the high Knudsen number simulation is repeated keeping  $[O_{3(g)}]$  constant at three different values. Peak  $[\operatorname{Cl}_2(g)]$  increases with increasing  $[O_{3(g)}]$  (Fig. 2) due to greater  $\operatorname{OH}_{(g)}$  becoming available from photolysis. There is, however, a subsequent fall in  $\operatorname{Cl}_{2(g)}$  concentration due to wall loss, and mass transfer of  $\operatorname{Cl}_{2(g)}$  into the droplet. Interface reaction (1) results in the droplets becoming alkaline, increasing the rate of  $\operatorname{Cl}_{2(g)}$  destruction via the aqueous-phase reaction,

$$Cl_{2(aq)} + OH_{(aq)}^{-} \rightarrow HOCl_{(aq)} + Cl_{(aq)}^{-}.$$
 (16)

Equilibrium between production of  $Cl_{2(g)}$  via interface reaction (1) and destruction via wall loss, mass transfer into the droplet and aqueous-phase reaction (16) prevents  $Cl_{2(g)}$  concentrations from reaching runaway levels despite the significantly higher amounts of available  $OH_{(g)}$ . In fact, in simulations with  $[O_{3(g)}]$  kept constant at relatively high levels of 10 and 100 ppmv (not shown here), similar qualitative behavior is observed.

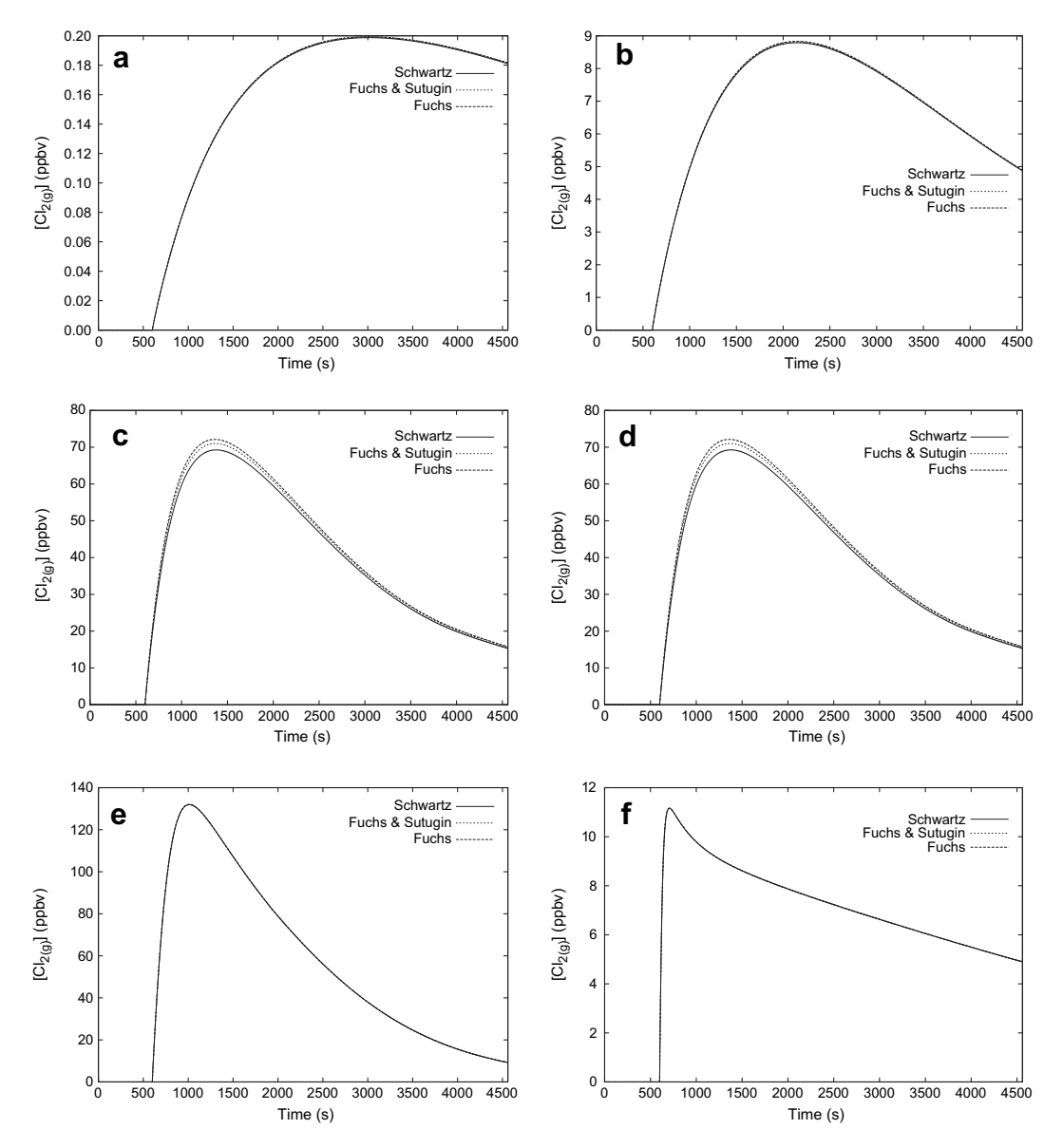


**Fig. 1.** Comparison of time evolution of  $Cl_{2(g)}$ , computed using Schwartz, Fuchs, and Fuchs & Sutugin mass-transfer expressions at three Knudsen numbers, (a) and (b) Kn = 0.01; (c) and (d) Kn = 0.60; and (e) and (f) Kn = 10. Total aerosol volume is kept constant across plots (a), (c) and (e). Total aerosol surface area is kept constant across plots (b), (d) and (f). Note that plots (c) and (d) are identical because they correspond to the base case with total aerosol volume and surface area being equal in both cases.

### 4.1.2. Constant total aerosol surface area

With total aerosol surface area held constant, the total aerosol volume is inversely proportional to Knudsen number and therefore decreases at higher Knudsen numbers. Consequently, at the kinetic regime Knudsen number, Kn=10 (Fig. 1f), there is less Cl $^-$  available to produce Cl<sub>2(g)</sub>. In contrast, at the continuum regime Knudsen number, Kn=0.01 (Fig. 1b) there is less Cl<sub>2(g)</sub> produced despite the greater amount of available Cl $^-$ . Maximum production of Cl<sub>2(g)</sub> occurs at the transition range Knudsen number, Kn=0.6 (Fig. 1d).

To explain this counterintuitive behavior, recall that the expression for interfacial reaction rate, Equation (13), written for interfacial reaction (1) between  $OH_{(g)}$  and  $Cl_{surface}^-$  is,

$$R_{\rm int} = \left(\frac{r^2}{3D_{\rm g}} + \frac{4r}{3\bar{\nu}\gamma}\right)^{-1} \left[OH_{\rm (g)}\right],\tag{17}$$

where the overall surface reaction probability for interface reaction (1),  $\gamma$ , is defined as,

$$\gamma = \phi \gamma' \beta_X \left[ \text{Cl}_{\text{surface}}^{-} \right]. \tag{18}$$

Here  $\beta_X[Cl_{surface}]$  is the fraction of droplet surface covered by chloride ions that have reached the interface.

The term in parentheses in Equation (17) can be considered an interfacial reaction rate constant. At low Knudsen numbers (large r) continuum regime mass transfer (first term in parentheses) dominates the interfacial reaction rate. This term increases as r increases, i.e., as Kn decreases. Hence the interfacial reaction rate decreases at low Knudsen numbers, leading to a decrease in peak  $\operatorname{Cl}_{2(g)}$  concentration. On the other hand, at high Knudsen numbers (small r) free-molecular mass transfer (second term in parentheses) dominates the interfacial reaction rate. This term, however, depends on the availability of  $\operatorname{Cl}^-$  at the surface. At high Kn,  $\operatorname{Cl}^-$  is significantly depleted owing to low total aerosol volume (Supplementary Fig. 3). Therefore, peak  $\operatorname{Cl}_{2(g)}$  concentration decreases at high Knudsen numbers.

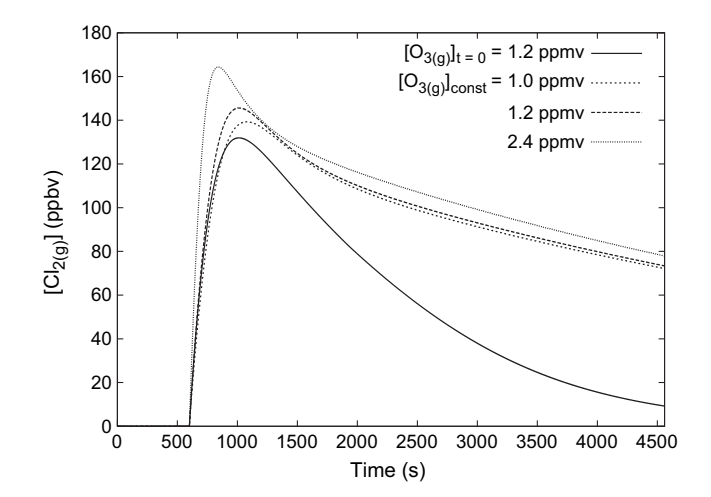


**Fig. 2.**  $\text{Cl}_{2(g)}$  concentration profiles computed at Kn=10, keeping  $O_{3(g)}$  concentration constant at three different levels. The solid line shows the profile computed with  $O_{3(g)}$  being consumed as the simulation progresses in time.

In comparing predictions using the three mass-transfer expressions, there is only a slight difference that is observed at the intermediate Knudsen number value, which lies in the transition regime. Overall, peak  $\text{Cl}_{2(g)}$  concentrations predicted using the different mass-transfer expressions differ by a maximum of 3%. This demonstrates that the model is relatively insensitive to the mass-transfer expression for  $\text{Cl}_{2(g)}$  production.

#### 4.2. Comparison of time evolution of $[Br_{2(g)}]$

The time evolution of  $[Br_{2(g)}]$  is studied for the same Knudsen numbers as in the NaCl particle scenario with only the particle concentrations different to correspond to experiments conducted by Hunt et al. (2004). Figs. 3 and 4 compare simulations using the three mass-transfer expressions at the lowest, intermediate, and highest values of Knudsen number, under dark and photolytic conditions respectively. These Knudsen numbers represent the continuum, transition, and kinetic regimes.

For NaBr aerosols, there are two different pathways for formation of gas-phase  $Br_{2(g)}$  via interfacial reaction. Interface reaction (2) is active only under photolytic conditions while interfacial reaction (3) is active under both dark and photolytic conditions. Additional pathways of  $Br_{2(g)}$  are available under photolytic conditions due to increased concentrations of photolytic products, complicating the system greatly. Simulations with dark conditions lack these competing pathways and hence are easier to understand compared to simulations with photolytic conditions.

# 4.2.1. Dark conditions

When the system is in the dark,  $Br_{2(g)}$  is produced primarily through interfacial reaction (3) (Hunt et al., 2004; Thomas et al., 2006, 2007; Nissenson et al., 2009). Additional bromine is produced in the aqueous-phase as a result of  $O_{3(g)}$  dissolving into the aerosols and undergoing the following reactions:

$$O_{3(aq)} + Br_{(aq)}^{-} \rightarrow BrO_{(aq)}^{-} + O_{2(aq)}$$
 (19)

$$BrO_{(aq)}^{-} + H_{(aq)}^{+} \rightleftharpoons HOBr_{(aq)}$$
 (20)

$$HOBr_{(aq)} + Br_{(aq)}^{-} + H_2O \rightarrow Br_{2(aq)} + OH_{(aq)}^{-} + H_2O.$$
 (21)

Aqueous-phase bromine produced by reaction (21) transfers to the gas-phase.

Fig. 3a, c, and e shows almost two orders of magnitude increase in peak  $[Br_{2(g)}]$  as the Knudsen number is increased from Kn=0.01 to Kn=10. Total aerosol volume is kept constant across these simulations, resulting in an increasing amount of surface area becoming available for interfacial reaction (3). For Kn=0.01 and Kn=0.55, the interfacial reaction is slow enough that peak  $[Br_{2(g)}]$  is not reached for the duration of the simulation and gas-phase  $Br_{2(g)}$  concentrations continue to increase monotonically. At the highest Knudsen number however, there is a peak and a subsequent fall-off that suggests a trend toward complete consumption of available  $O_3$  by interfacial reaction (3).

With total aerosol surface area held constant, total aerosol volume decreases at higher Knudsen numbers. Peak  $[Br_{2(g)}]$ , however, decreases only by a factor of 2, as the Knudsen number is increased from Kn=0.01 to Kn=0.55 and further to Kn=10 (Fig. 3b, d, and f). This is due to the relative importance of interfacial reaction (3) compared to aqueous-phase reaction mechanisms in producing  $Br_{2(g)}$ .

#### 4.2.2. Photolytic conditions

Under photolytic conditions, many new chemical pathways are available due to the presence of hydroxyl radicals produced by photolysis of ozone via reactions (4) and (5). Hydroxyl radicals affect the concentration of bromine directly through interfacial reaction (2) and by reacting with  $Br_{2(g)}$ , producing  $HOBr_{(g)}$  and  $Br_{(g)}$ . In addition, hydroxyl radicals may also react with other gasphase species and indirectly affect  $Br_{2(g)}$  concentrations. A modeling study by Thomas et al. (2006); Thomas et al. (2007) demonstrates that Br<sub>2(g)</sub> is produced rapidly when NaBr aerosols in the transition regime are irradiated in the presence of ozone. Including interfacial reaction (2) produces only moderate increases in the concentration of  $Br_{2(g)}$ . Numerous studies have shown that rapid production of Br<sub>2(g)</sub> can result from a complex mechanism involving gas-phase chemistry, aqueous-phase chemistry, and mass transfer (Fan and Jacob, 1992; Tang and McConnell, 1996; Fickert et al., 1999; Foster et al., 2001; Adams et al., 2002; Huff and Abbatt, 2002; Nissenson et al., 2009),

$$Br_{2(g)} + h\nu \rightarrow 2Br_{(g)} \tag{22}$$

$$Br_{(g)} + O_{3(g)} \rightarrow BrO_{(g)} + O_{2(g)}$$
 (23)

$$2BrO_{(g)} \rightarrow 2Br_{(g)} + O_{2(g)}$$
 (24)

$$2BrO_{(g)} \rightarrow Br_{2(g)} + O_{2(g)}$$
 (25)

$$BrO_{(g)} + HO_{2(g)} \rightarrow HOBr_{(g)} + O_{2(g)}$$
 (26)

$$HOBr_{(g)} \rightarrow HOBr_{(aq)}$$
 (27)

$$HOBr_{(aq)} \ + \ Br_{(aq)}^{-} \ + \ H_{2}O \ \rightarrow \ Br_{2(aq)} \ + \ OH_{(aq)}^{-} \ + \ H_{2}O. \eqno(21)$$

Aqueous-phase  $Br_2$  produced in reaction (21) transfers out of the droplet. Note that one bromine atom in the form of  $HOBr_{(aq)}$  enters the droplet but two bromine atoms in the form of  $Br_{2(g)}$  leave the droplet. This allows for rapid release of bromine from the droplets, causing a so-called "bromine explosion" in the gas-phase.

A rapid depletion of ozone resulting from photolysis and catalytic destruction by  $Br_{(g)}$  and  $BrO_{(g)}$  through reactions (22)–(26) occurs simultaneously with this explosion of bromine upon illumination with UV light (Fig. 5). Loss of significant amounts of ozone in the system halts further bromine production since the most important mechanisms of  $Br_{2(g)}$  production are dependent

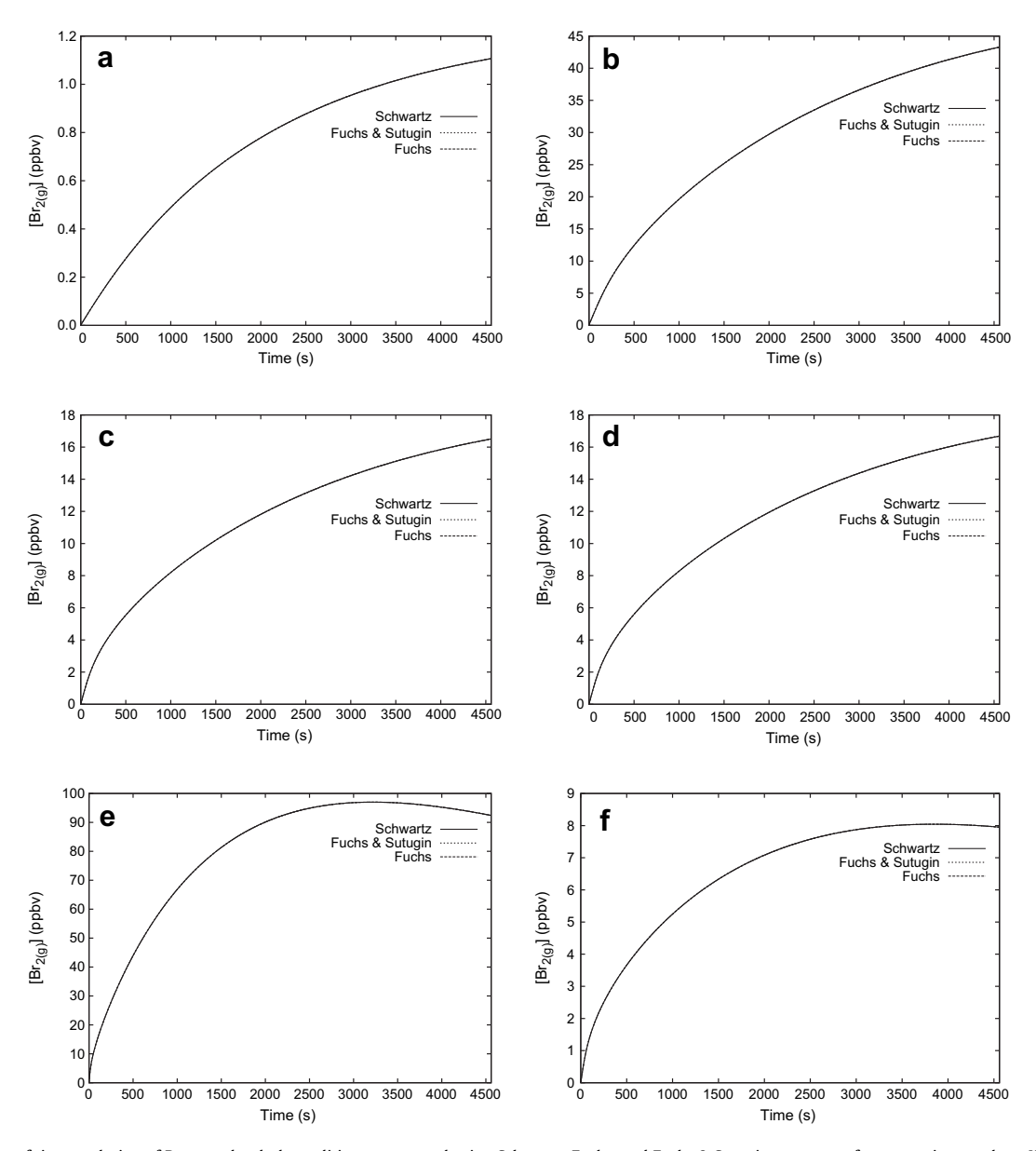


**Fig. 3.** Comparison of time evolution of  $Br_{2(g)}$  under dark conditions, computed using Schwartz, Fuchs, and Fuchs & Sutugin mass-transfer expressions at three Knudsen numbers, (a) and (b) Kn = 0.01; (c) and (d) Kn = 0.55; and (e) and (f) Kn = 10. Total aerosol volume is kept constant across plots (a), (c) and (e). Total aerosol surface area is kept constant across plots (b), (d) and (f). Note that plots (c) and (d) are identical because they correspond to the base case with total aerosol volume and surface area being equal in both cases.

upon ozone levels. The bromine explosion described in reactions (21)–(27) is dependent upon the rate of mass transfer of HOBr (into the aqueous-phase) and of Br<sub>2</sub> (out of the aqueous-phase) and, therefore, is dependent upon the total aerosol surface area available.

Fig. 4a, c and e shows  $Br_{2(g)}$  production at three Knudsen numbers corresponding to the continuum, transition and kinetic regimes respectively. Total aerosol volume is held constant across these simulations. There is very little  $Br_{2(g)}$  produced in the continuum regime (Kn=0.01) due to the limited surface area available. Most of the  $Br_{2(g)}$  is produced in the dark and is lost to the walls and to the droplets.  $OH_{(g)}$  produced by photolysis is consumed rapidly before it can produce  $Br_{2(g)}$  via interfacial reaction (2). At transition and kinetic range Knudsen numbers (Kn=0.55,10) a much greater amount of  $Br_{2(g)}$  is produced by the bromine explosion mechanism, reactions (21)–(27). The importance of interfacial reaction (3) in producing  $Br_{2(g)}$  during the 600 s

dark period increases with increasing surface area at higher Knudsen numbers. Additionally, this results in less  $O_{3(g)}$  being available for photolysis to  $OH_{(g)}$ .

With total aerosol surface area held constant,  $Br_{2(g)}$  production decreases with increasing Knudsen number due to a decrease in total aerosol volume. Fig. 4b, d and f shows  $Br_{2(g)}$  production at three Knudsen numbers corresponding to the continuum, transition and kinetic regimes respectively.  $Br^-$  depletion at high Knudsen numbers, due to the low volume in the system, leads to a decrease in the rate of aqueous-phase reaction (21). This reduces  $Br_{2(g)}$  production via the bromine explosion pathway. Supplementary Fig. 4 shows a trend towards complete consumption of  $Br^-$  at higher Knudsen numbers. In the kinetic regime (Kn=10), Fig. 4f,  $Br_{2(g)}$  is produced only during a short time span due to  $Br^-$  depletion.

When comparing predictions obtained using the three different mass-transfer expressions,  $Br_{2(g)}$  is less sensitive than  $Cl_{2(g)}$  to the mass-transfer expression employed. As seen in Figs. 3 and 4, the

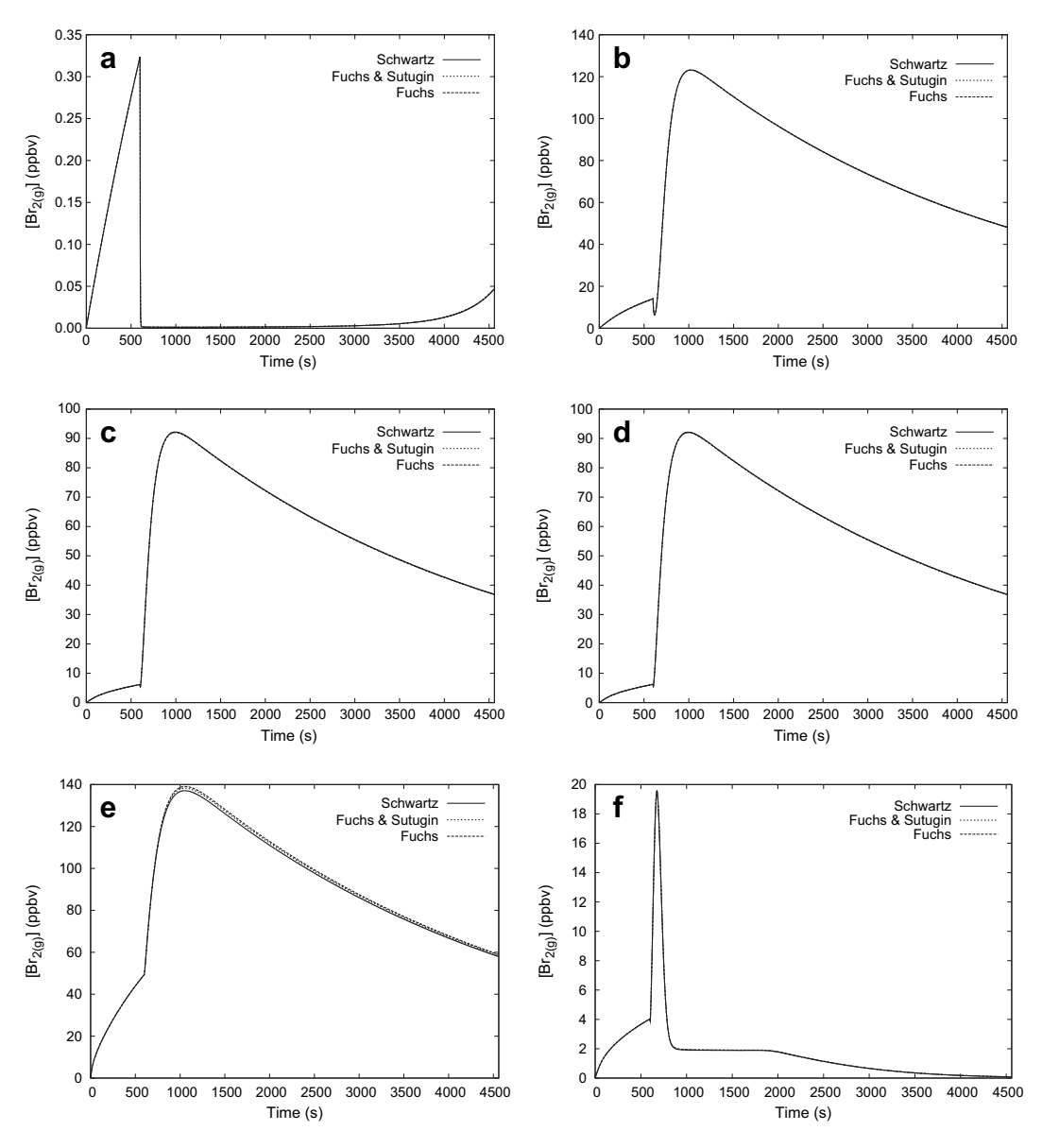
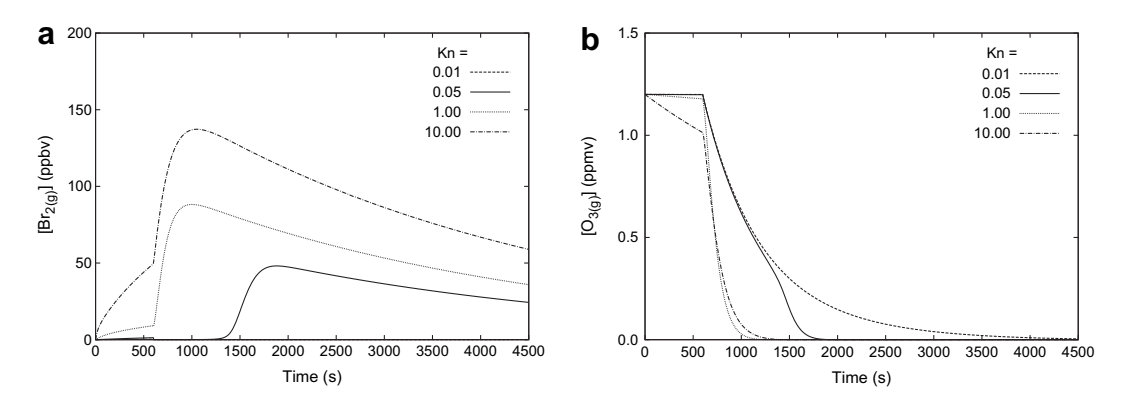
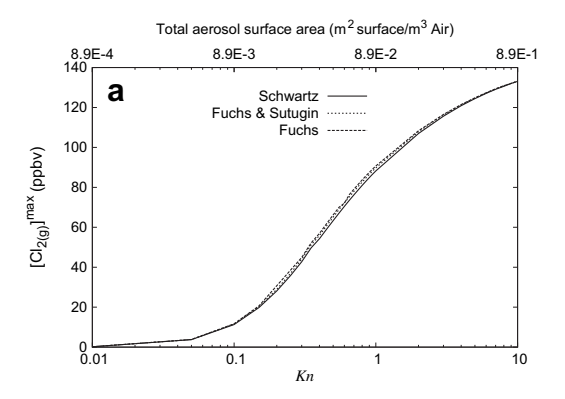


Fig. 4. Comparison of time evolution of  $Br_{2(g)}$  under photolytic conditions, computed using Schwartz, Fuchs, and Fuchs & Sutugin mass-transfer expressions at three Knudsen numbers, (a) and (b) Kn = 0.01; (c) and (d) Kn = 0.55; and (e) and (f) Kn = 10. Lights are turned on at 600 s. Total aerosol volume is kept constant across plots (a), (c) and (e). Total aerosol surface area is kept constant across plots (b), (d) and (f). Note that plots (c) and (d) are identical because they correspond to the base case with total aerosol volume and surface area being equal in both cases.



 $\textbf{Fig. 5.} \ \ \text{Time evolution of Br}_{2(g)} \ \ \text{and } O_{3(g)} \ \ \text{concentrations at selected Knudsen numbers for NaBr aerosols under photolytic conditions, using the Schwartz mass-transfer expression.}$ 



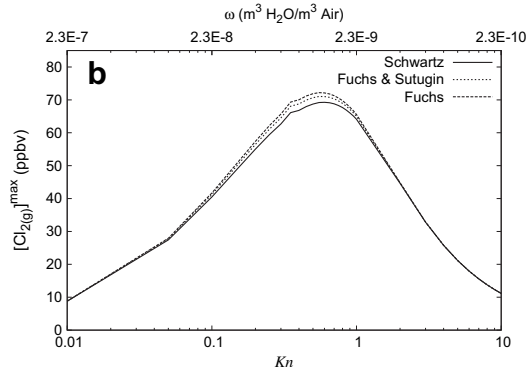


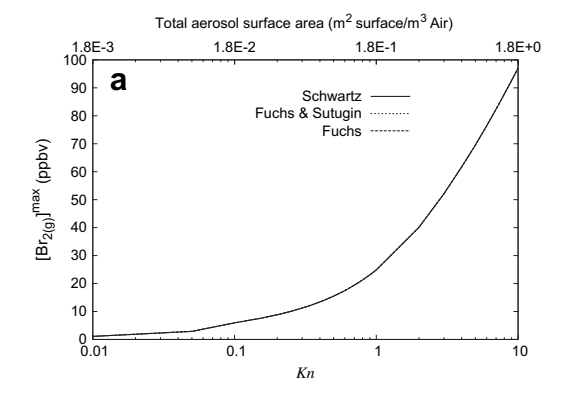
Fig. 6. Peak  $Cl_{2(g)}$  concentrations as a function of Knudsen number, computed using three mass-transfer expressions. Peak concentrations are obtained from transient simulations that predict time evolution of  $[Cl_{2(g)}]$ . Total aerosol volume is held constant in plot (a), with total aerosol surface area shown on the top axis. Total aerosol surface area is held constant in plot (b), with liquid water content ( $\omega$ ) shown on the top axis.

predictions are almost identical at all the Knudsen numbers considered here. Differences in peak  $Br_{2(g)}$  concentrations are just a fraction of a percent over the entire range.

### 4.3. Knudsen number dependence of peak $[Cl_{2(g)}]$ and $[Br_{2(g)}]$

Peak values of gas-phase Cl<sub>2</sub> and Br<sub>2</sub> concentrations are obtained from transient simulations over the range of Knudsen numbers and particle concentrations presented in Tables 1 and 2. Fig. 6 shows  $[Cl_{2(g)}]^{max}$  as a function of Kn, predicted using the three mass-transfer expressions. With total aerosol volume held constant, the peak tends towards an asymptotic maximum at high Kn (Fig. 6a). The maximum [Cl<sub>2(g)</sub>] that can be produced is limited by the amount of ozone initially available for photolysis to  $OH_{(g)}$ . With increasing surface area becoming available for interfacial reaction (1) at higher Knudsen numbers, the peak value is reached much faster than at lower Knudsen numbers, with more  $OH_{(g)}$ being consumed at the interface. With total aerosol surface area held constant,  $[Cl_{2(g)}]^{max}$  peaks in the transition regime and decreases both in the continuum and kinetic regimes (Fig. 6b). This is due to a decrease in Cl<sup>-</sup> available at the interface with increasing Kn. Interfacial reaction (1) being the dominant source of gas-phase Cl<sub>2</sub>, the relative contributions of the kinetic and continuum regime mass-transfer rates to the total interface reaction rate (Equation 17) are important to understanding the trend in  $[\text{\rm Cl}_{2(g)}]^{max}$  with Knudsen number. Supplementary Fig. 5 compares the magnitudes of the two terms in Equation (17) over the range of Knudsen numbers examined. The terms are computed at a simulation time corresponding to  $[{\rm Cl}_{2(g)}]^{\rm max}$ . There is a diffusion limitation at low Kn due the dominance of the diffusion mass-transfer term  $(r^2/3D_g)$ . This leads to a decrease in  $[{\rm Cl}_{2(g)}]^{\rm max}$  from the transition regime to the continuum regime.

In contrast to  $Cl_{2(g)}$  production where the interface reaction is dominant, aqueous-phase reaction mechanisms also play an important role in the production of  $Br_{2(g)}$  from NaBr aerosols both in the dark and under photolytic conditions (Nissenson et al., 2009). Fig. 7 shows  $[Br_{2(g)}]^{max}$  as a function of Knudsen number using the three mass-transfer expressions under dark conditions. In this case. interfacial reaction (3) is the only surface area dependent reaction mechanism. Therefore, with total aerosol volume held constant, [Br<sub>2(g)</sub>]<sup>max</sup> increases with Knudsen number due to greater surface area becoming available for interfacial reaction (Fig. 7a). With the total aerosol surface area held constant, it is expected that the bulk reaction mechanisms will determine the trends in peak Br<sub>2(g)</sub> with Knudsen number. The decrease in peak concentrations with Knudsen number (Fig. 7b) is a direct consequence of the decrease in total aerosol volume. At higher Knudsen numbers, less Br is available in the droplets (Supplementary Fig. 3) to produce Br<sub>2(g)</sub> via aqueous-phase reaction (21). Although interfacial reaction (3) is the dominant source of gas-phase Br2 under dark conditions, a monotonic decrease in  $[Br_{2(g)}]^{max}$  with  $\mathit{Kn}$  is observed, in contrast to gas-phase  $[Cl_{2(g)}]^{max}$  which peaks in the transition regime. Supplementary Fig. 6 compares magnitudes of the kinetic and continuum regime mass-transfer rates over the entire range of Knudsen number. These terms are computed at the end of the simulation when  $[Br_{2(g)}]$  is maximal. In contrast to the  $Cl_{2(g)}$  case,



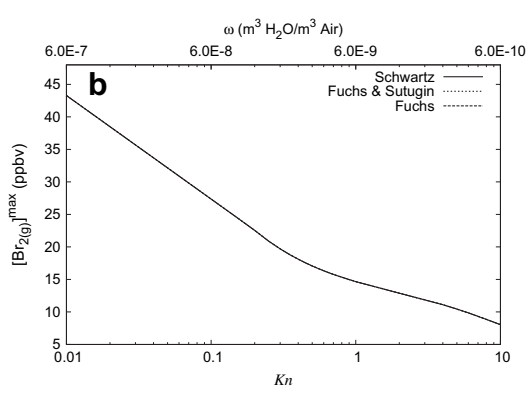


**Fig. 7.** Peak  $Br_{2(g)}$  concentrations as a function of Knudsen number, computed using three mass-transfer expressions under dark conditions. Peak concentrations are obtained from transient simulations that predict time evolution of  $[Br_{2(g)}]$ . Total aerosol volume is held constant in plot (a), with total aerosol surface area shown on the top axis. Total aerosol surface area is held constant in plot (b), with liquid water content ( $\omega$ ) shown on the top axis.

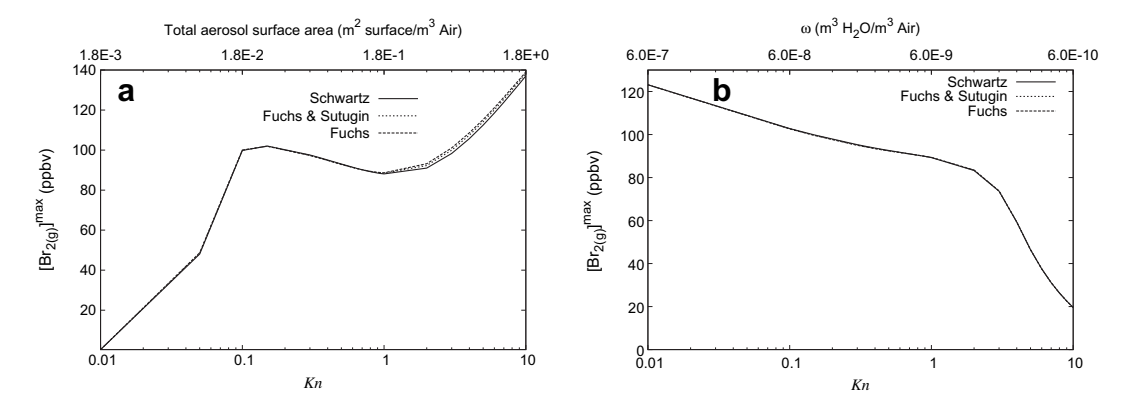


**Fig. 8.** Peak  $Br_{2(g)}$  concentrations as a function of Knudsen number, computed using three mass-transfer expressions under photolytic conditions. Peak concentrations are obtained from transient simulations that predict time evolution of  $[Br_{2(g)}]$ . Total aerosol volume is held constant in plot (a), with total aerosol surface area shown on the top axis. Total aerosol surface area is held constant in plot (b), with liquid water content ( $\omega$ ) shown on the top axis.

there is no diffusion limitation here and the kinetic term dominates at all Knudsen numbers.

Fig. 8 shows  $[Br_{2(g)}]^{max}$  as a function of Knudsen number for NaBr aerosols under photolytic conditions. With total aerosol volume held constant, the changing surface area affects competition for ozone in the production of bromine between bromine explosion in reactions (21)–(27), interfacial reactions (2) and (3), and aqueous-phase production via reactions (19)–(21). This leads to an inflection point in the transition regime (Fig. 8a). As Knudsen number increases in the continuum regime, peak bromine concentration increases as more surface area becomes available for mass transport of HOBr and Br<sub>2</sub>, hastening the onset of the bromine explosion. In the kinetic regime, the increased surface area results in interfacial reaction (3) gaining importance in bromine production. Peak bromine increases with Knudsen number in this regime because the interfacial reaction occurs rapidly before the onset of ozone photolysis and catalytic destruction of ozone by reactions (22)–(25) at 600 s. As Kn increases further, peak  $Br_{2(g)}$  concentration approaches an asymptotic limit (on a linear scale, the bromine concentration curve appears logarithmic). With total aerosol surface area held constant, aqueous-phase production via reactions (19)–(21) dominates at low Knudsen numbers where total aerosol volume available is greatest. Fig. 8b shows a monotonic decrease in  $[Br_{2(g)}]^{max}$  with Knudsen number due to decreasing aerosol volume.

#### 5. Conclusions

Three different mass-transfer expressions have been implemented in MAGIC. Simulations have been performed of gas-phase Cl<sub>2</sub> and Br<sub>2</sub> production from NaCl and NaBr aerosols respectively. Simulations have been performed of NaCl aerosols reacting with ozone in the presence of UV light. In the case of NaBr aerosols, both dark and photolytic conditions have been investigated. A range of Knudsen numbers spanning the continuum, transition and free-molecular regimes has been considered. While all situations are relatively insensitive to the mass-transfer expression used, useful insights are gained into the production of gas-phase species from aerosol particles via different bulk and interfacial reaction mechanisms. The relative importance of these mechanisms is investigated over a range of atmospherically relevant Knudsen numbers by keeping (a) total aerosol volume and (b) total aerosol surface area constant.

With total aerosol volume held constant, total aerosol surface area increases linearly with Knudsen number while overall contribution from aqueous-phase chemistry remains constant. Peak gas-phase  $\text{Cl}_2$  increases by two orders of magnitude when going from the continuum regime to the kinetic regime. This increase is due to greater surface area becoming available at higher Knudsen numbers leading to a heightened dominance of the interfacial reaction between gas-phase OH and surface chloride ions. However, the peak value at high Knudsen numbers is limited by the initial amount of gas-phase  $\text{O}_3$  available to be photolyzed to OH. At low Knudsen numbers, production of  $\text{Cl}_{2(g)}$  is greatly reduced due to reduced surface area, suppressing the interfacial reaction. Contribution from bulk aqueous-phase chemistry remains insignificant at all Knudsen numbers.

Under dark conditions,  $Br_{2(g)}$  concentration varies by two orders of magnitude over the range of Knudsen numbers considered. The increase in concentration with Knudsen number is due to the increased surface area available for interfacial reaction between ozone and surface bromide ions. The limit of  $[\text{Br}_{2(g)}]^{\text{max}}$  dependent on initial O<sub>3</sub> available for interfacial reaction is not reached for the range of Knudsen numbers studied here. Under photolytic conditions, bromide ions react at the surface with both ozone and gasphase OH. In addition to competition between the two interfacial reactions, gas-phase chemistry, aqueous-phase chemistry, and mass transport processes also contribute to the production of  $Br_{2(g)}$ . There is significantly more  $Br_{2(g)}$  produced in the transition regime under photolytic conditions, compared to that produced under dark conditions, due to the bromine explosion pathway. At higher Knudsen numbers, i.e., in the free-molecular regime, this difference is reduced, although more bromine is still produced under photolytic conditions.

With total aerosol surface area held constant, total aerosol volume is inversely proportional to  $\mathit{Kn}$ . At high Knudsen numbers, depletion in  $Cl^-$  available for interfacial reaction leads to a decrease in  $Cl_{2(g)}$  production. Maximum gas-phase  $Cl_2$  is produced in the transition regime under these conditions due to a diffusion limitation in the continuum regime. In the case of  $Br_{2(g)}$  production from NaBr aerosols, aqueous-phase reaction mechanisms determine the trends with Knudsen number. Gas-phase  $Br_2$  decreases monotonically under both dark and photolytic conditions due to lesser aerosol volume being available at higher Knudsen numbers. More  $Br_{2(g)}$  is produced under photolytic conditions than under dark conditions at all Knudsen numbers.

#### Acknowledgements

This work was supported by grant CHE-0431312 from the United States National Science Foundation.

#### Appendix. Supplementary material

Supplementary data associated with this article can be found, in the online version, at doi:10.1016/j.atmosenv.2009.10.014.

#### References

- Adams, J.W., Holmes, N.S., Crowley, J.N., 2002. Uptake and reaction of HOBr on frozen and dry salt surfaces. Atmospheric Chemistry and Physics 2, 79–91.
- DeHaan, D.O., Brauers, T., Oum, K.W., Stutz, J., Nordmeyer, T., Finlayson-Pitts, B.J., 1999. Heterogeneous chemistry in the troposphere: experimental approaches and applications to the chemistry of sea salt particles. International Reviews in Physical Chemistry 18, 343–385.
- Fan, S.M., Jacob, D.J., 1992. Surface ozone depletion in arctic spring sustained by bromine reactions on aerosols. Nature 359, 522–524.
- Fickert, S., Adams, J.W., Crowley, J.N., 1999. Activation of  ${\rm Br_2}$  and BrCl via uptake of HOBr onto aqueous salt solutions. Journal of Geophysical Research 104, 23719–23727.
- Finlayson-Pitts, B.J., Pitts Jr., J.N., 2000. Chemistry of the Upper and Lower Atmosphere Theory, Experiments and Applications. Academic Press, San Diego, USA.
- Foster, K.L., Plastridge, R.A., Bottenheim, J.W., Shepson, P.B., Finlayson-Pitts, B.J., Spicer, C.W., 2001. The role of Br<sub>2</sub> and BrCl in surface ozone destruction at polar sunrise. Science 291, 471–474.
- Fuchs, N.A., 1964. Mechanics of Aerosols. Pergamon Press, New York, USA.
- Fuchs, N.A., Sutugin, G.A., 1971. Topics in Current Aerosol Research. Pergamon, New York, pp. 1–60.
- von Glasow, R., Sander, R., Bott, A., Crutzen, P.J., 2002. Modeling halogen chemistry in the marine boundary layer 1. Cloud-free MBL. Journal of Geophysical Research 107 (D17), 4341–4356.
- Hu, J.H., Shi, Q., Davidovits, P., Worsnop, D.R., Zahniser, M.S., Kolb, C.E., 1995. Reactive uptake of  $Cl_{2(g)}$  and  $Br_{2(g)}$  by aqueous surfaces as a function of  $Br^-$  and  $I^-$  ion concentration: the effect of chemical reaction at the interface. Journal of Physical Chemistry 99, 8768–8776.
- Huff, A.K., Abbatt, J.P.D., 2002. Kinetics and product yields in the heterogeneous reactions of HOBr with ice surfaces containing NaBr and NaCl. Journal of Physical Chemistry A 106, 11559–11572.
- Hunt, S.W., Roeselova, M., Wang, W., Wingen, L.M., Knipping, E.M., Tobias, D.J., Dabdub, D., Finlayson-Pitts, B.J., 2004. Formation of molecular bromine from the reaction of ozone with deliquesced NaBr aerosol: evidence for interface chemistry. Journal of Physical Chemistry A 108, 11559–11572.
- Jacob, D.J., 2000. Heterogeneous chemistry and tropospheric ozone. Atmospheric Environment 34, 2131–2159.
- Knipping, E.M., Dabdub, D., 2002. Modeling Cl<sub>2</sub> formation from aqueous NaCl particles: evidence for interfacial reactions and importance of Cl<sub>2</sub> decomposition in alkaline solution. Journal of Geophysical Research 107, 4360–4389.

- Knipping, E.M., Dabdub, D., 2003. Impact of chlorine emissions from sea-salt aerosol on coastal urban ozone. Environmental Science and Technology 37 (2), 275–284.
- Knipping, E.M., Lakin, M.J., Foster, K.L., Jungwirth, P., Tobias, D.J., Gerber, R.B., Dabdub, D., Finlayson-Pitts, B.J., 2000. Experiments and simulations of ionenhanced interfacial chemistry on aqueous NaCl aerosols. Science 288, 301–306.
- Nissenson, P., Thomas, J.L., Finlayson-Pitts, B.J., Dabdub, D., 2008. Sensitivity and uncertainty analysis of the mechanism of gas-phase chlorine production from NaCl aerosols in the MAGIC model. Atmospheric Environment 42 (29), 6934–6941.
- Nissenson, P., Packwood, D., Hunt, S.W., Finlayson-Pitts, B.J., Dabdub, D., 2009. Probing the sensitivity of gaseous Br<sub>2</sub> production from the oxidation of aqueous bromide-containing aerosols and atmospheric implications. Atmospheric Environment 43, 3951–3962.
- Oum, K.W., Lakin, M.J., DeHaan, D.O., Brauers, T., Finlayson-Pitts, B.J., 1998. Formation of molecular chlorine from the phytolysis of ozone and aqueous sea salt particles. Science 279, 74–77.
- Pandis, S.N., Seinfeld, J.H., 1989. Sensitivity analysis of a chemical mechanism for aqueous-phase atmospheric chemistry. Journal of Geophysical Research 29 (D1), 1105—1126.
- Piot, M., von Glasow, R., 2008. The potential impact of frost flowers, recycling on snow, and open leads for ozone depletion events. Atmospheric Chemistry and Physics 8, 2437–2467.
- Read, K.A., Mahajan, A.S., Carpenter, L.J., Evans, M.J., Faria, B.V.E., Heard, D.E., Hopkins, J.R., Lee, J.D., Moller, S.J., Lewis, A.C., Mendes, L., McQuaid, J.B., Oetjen, H., Saiz-Lopez, A., Pilling, M.J., Plane, J.M.C., 2008. Extensive halogenmediated ozone destruction over the tropical Atlantic Ocean. Nature 453, 1232–1235.
- Sahni, D.C., 1966. The effect of a black sphere on the flux distribution of an infinite moderator. Journal of Nuclear Energy 20, 915—920.
- Sander, R., 1999. Modeling atmospheric chemistry: interactions between gas-phase species and liquid cloud/aerosol particles. Surveys in Geophysics 20, 1–31.
- Schwartz, S.E., 1986. Mass-transport considerations pertinent to aqueous-phase reactions of gases in liquid-water clouds. In: Jaeschke, W. (Ed.), Chemistry of Multiphase Atmospheric Systems. NATO ASI Series, vol. G6. Springer-Verlag, New York.
- Seinfeld, J.H., Pandis, S.N., 1998. Atmospheric Chemistry and Physics: From Air Pollution to Climate Change. Wiley-Interscience, New York, USA.
- Tang, T., McConnell, J.C., 1996. Autocatalytic release of bromine from arctic snow pack during polar sunrise. Geophysics Research Letters 23, 2633–2636.
- Thomas, J.L., Jimenez-Aranda, A., Finlayson-Pitts, B.J., Dabdub, D., 2006. Gas-phase molecular halogen formation from NaCl and NaBr aerosols: when are interface reactions important? Journal of Physical Chemistry A 110, 1859–1867.
- Thomas, J.L., Jimenez-Aranda, A., Finlayson-Pitts, B.J., Dabdub, D., 2007. Gas-phase molecular halogen formation from NaCl and NaBr aerosols: when are interface reactions important? Journal of Physical Chemistry A 110, 1859–1867. Erratum 111, 7243–7244.